Natural Convection in a Wedge-Shaped Domain Induced by Constant Isothermal Surface Heating

Chengwang Lei[1], Yadan Mao[2] and John C. Patterson[1]

[1]School of Civil Engineering
The University of Sydney, Sydney, NSW 2006, Australia

[2]Institute of Geophysics and Geomatics
China University of Geosciences, China

Abstract

The present investigation is concerned with natural convection in a wedge-shaped domain induced by constant isothermal heating at the water surface. A semi-analytical approach coupled with scaling analysis and numerical simulation is adopted to resolve the problem. The study reveals that the overall flow domain in the wedge is composed of two distinct sub-regions, a conductive region near shore and a convective region offshore. The major time and velocity scales governing the flow development in both regions are proposed and verified.

Introduction

Convective circulations in coastal waters induced by heat transfer through the water surface play an important role in the transport of nutrients, pollutants and chemical species across reservoirs and lakes, and thus have attracted significant research interest (see for example [1-3]). Over a typical diurnal cycle, the water body is subject to heating by solar radiation in the daytime and cooling by heat loss through the water surface at the night-time. The problem of constant heating by solar radiation has been investigated in [4-6], and that of constant cooling by heat loss from the surface has been investigated in [7-9]. The problem of alternate heating and cooling over diurnal cycles has also been reported in [3, 10, 11]. Almost all of the existing investigations on this topic have considered an iso-flux thermal boundary condition at the water surface, either in the form of uniform radiation entering the water body or a uniform heat flux leaving the water body.

In the absence of solar radiation, the water bodies are also subject to heating or cooling due to the temperature difference between the water bodies and the atmosphere. The proper thermal boundary condition relevant to this situation would be a prescribed temperature rather than a heat flux at the water surface. Unfortunately, studies of heating or cooling by an isothermal surface temperature are very scarce. The only studies reported in the literature seem to be the experimental works of Bednarz et al. [12, 13]. In [12], a constant temperature which is lower than the initial water temperature is imposed at the water surface to model the night-time cooling problem. In the more recent experiment reported in [13], the water surface temperature is altered periodically in order to model the diurnal thermal cycle.

A literature survey indicates that no analytical solution or theoretical analysis is yet available to quantify the flow properties in coastal waters subject to isothermal heating or cooling. This has motivated the present investigation. In this study, a hybrid of asymptotic solution and scaling analysis is developed to quantify the flow properties in coastal waters. Numerical simulations are also conducted to verify the asymptotic solution and scaling relations.

The Physical Model and Numerical Procedures

Under consideration is a two-dimensional (2D) wedge-shaped domain consisting of a near-shore region with a sloping bottom (the slope is A) and an offshore region with a uniform depth, as depicted in figure 1. The maximum water depth in the model reservoir is h. Initially the water is stationary and isothermal at a temperature of T_0 throughout the entire domain. At the start-up, a uniform temperature $T_0+\Delta T$ is imposed at the water surface and maintained thereafter. The subsequent development of the natural convection flow in the wedge is governed by the following 2D Navier-Stokes and energy equations, in which the usual Boussinesq assumption has been made:
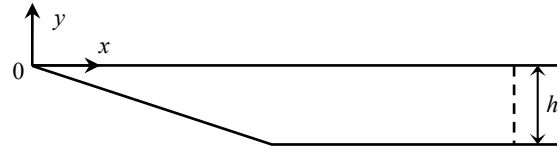

Figure 1. Sketch of the flow domain and the coordinate system.

$$\frac{\partial u}{\partial x} + \frac{\partial v}{\partial y} = 0 \qquad (1)$$

$$\frac{\partial u}{\partial t} + u\frac{\partial u}{\partial x} + v\frac{\partial u}{\partial y} = -\frac{1}{\rho_0}\frac{\partial p}{\partial x} + \nu\nabla^2 u \qquad (2)$$

$$\frac{\partial v}{\partial t} + u\frac{\partial v}{\partial x} + v\frac{\partial v}{\partial y} = -\frac{1}{\rho_0}\frac{\partial p}{\partial y} + \nu\nabla^2 v + g\beta(T - T_0) \qquad (3)$$

$$\frac{\partial T}{\partial t} + u\frac{\partial T}{\partial x} + v\frac{\partial T}{\partial y} = k\nabla^2 T \qquad (4)$$

where u and v are the velocity components in the x and y-directions respectively; t is the time; p is the pressure; T is the temperature; g is the gravitational acceleration; and ρ_0, ν, β, k are the density, kinematic viscosity, thermal expansion coefficient and thermal diffusivity of water at the reference temperature T_0.

A rigid non-slip and adiabatic boundary condition ($u = v = 0$ and $\partial T/\partial n = 0$ where n is the direction normal to the bottom) is assumed for the sloping and flat bottoms. The water surface is stress free ($\partial u/\partial y = 0$ and $v = 0$). An open boundary condition is considered at the deep end ($\partial T/\partial x = 0$, $\partial u/\partial x = 0$ and $v = 0$), and any backflow from the deep end is at the reference temperature of T_0.

Before solving the governing equations numerically, equations (1)-(4), along with the above-described initial and boundary conditions, are normalised using the following characteristic scales: the length scale $x, y \sim h$; the time scale $t \sim h^2/k$; the velocity scale $u, v \sim k/h$; the pressure gradient scale p_x, $p_y \sim \rho g\beta\Delta T$; and the temperature difference scale $[T-(T_0+\Delta T)] \sim \Delta T$. The resultant normalised governing equations are characterised by two non-dimensional parameters: the Prandtl

(Pr) and Rayleigh (Ra) numbers, which are defined as

$$Pr = \frac{\nu}{\kappa}, \qquad Ra = \frac{g\beta\Delta T h^3}{\nu\kappa} \tag{5}$$

The normalized governing equations are solved numerically using a finite-volume method. In all simulations, the maximum dimensionless water depth is 1; the sloping and flat regions are of the same length; and a fixed Prandtl number of $Pr = 7$ is adopted. Two bottom slopes of $A = 0.05$ and 0.1 respectively are calculated. The flow domain is meshed with a non-uniform grid which has an increasing grid density toward all of the boundaries. Mesh and time-step dependency tests have been conducted for a typical case in the convective flow regime with a Rayleigh number $Ra = 2 \times 10^7$ using three different meshes of 301×51, 451×75 and 601×101 respectively. Based on these tests, the medium grid 451×75 is adopted in the subsequent simulations, and the corresponding dimensionless time step is 2.0×10^{-4}.

Theoretical Analysis and Numerical Validation

For the model described above, it is expected that, at any time $t > 0$, the entire domain consists of two distinct sub-regions, one near the tip with a uniform temperature – a conductive region; and the other further out of the tip with a distinct thermal boundary layer. There will also be a transitional region between these two distinct sub-regions.

Analysis and Simulation for the Conductive Region

After the isothermal heating is initiated at the water surface, heat is transferred to the interior by conduction, resulting in a horizontal thermal boundary layer growing downwards from the surface. The scale for the thermal boundary layer thickness can be derived from a balance between the unsteady and vertical diffusion terms in the energy equation (4) as (refer to [14])

$$\delta_T \sim (kt)^{1/2} \tag{6}$$

The heat transfer process at the early stage can be simplified as a one-dimensional (1D) vertical conduction problem with a variable local water depth of Ax, and described by the following 1D equation

$$\frac{\partial T}{\partial t} = k\frac{\partial^2 T}{\partial y^2} \tag{7}$$

The above described initial and boundary conditions are also applicable to the 1D conduction problem, which can be solved by separation of variables. The solution of temperature is

$$T = T_0 + \Delta T - \sum_{n=0}^{\infty} \frac{4\Delta T}{(2n+1)\pi} e^{-\frac{(n+\frac{1}{2})^2 \pi^2 kt}{A^2 x^2}} \sin\left(n+\frac{1}{2}\right)\pi\frac{y}{Ax} \tag{8}$$

The average temperature over the local depth at a given offshore distance x can be calculated as

$$\overline{T} = \frac{1}{Ax}\int_{-Ax}^{0} T dy = T_0 + \Delta T - \sum_{n=0}^{\infty} \frac{8\Delta T}{(2n+1)^2\pi^2} e^{-\frac{(n+1/2)^2\pi^2}{A^2 x^2}kt} \tag{9}$$

and the horizontal gradient of the local average temperature can be obtained as

$$\frac{\partial \overline{T}}{\partial x} = -\sum_{n=0}^{\infty} \frac{4\Delta T}{A^2 x^3} kt e^{-\frac{(n+1/2)^2\pi^2}{A^2 x^2}kt} \tag{10}$$

Since the summation terms in (10) decrease rapidly with n, the above summation can be approximated by the first term $n = 0$ as follows

$$\frac{\partial \overline{T}}{\partial x} \sim -\frac{4\Delta T}{A^2 x^3} kt e^{-\frac{\pi^2}{4A^2 x^2}kt} \tag{11}$$

After normalization (10) and (11) are rewritten as

$$\frac{\partial \overline{\tau}}{\partial x} = -\sum_{n=0}^{\infty} \frac{4}{A^2 x^3} te^{-\frac{(n+1/2)^2\pi^2}{A^2 x^2}t} \tag{12}$$

$$\frac{\partial \overline{\tau}}{\partial x} \sim -\frac{4}{A^2 x^3} te^{-\frac{\pi^2}{4A^2 x^2}kt} \tag{13}$$

The temperature gradient given in (13) is a function of both time and offshore distance, and thus can be examined from both temporal and spatial perspectives. From the temporal perspective, the time at which the first derivative of the horizontal temperature gradient with respect to time approaches zero represents the time when the maximum temperature gradient occurs at a given position x. This time is derived using (13) as

$$t_m \sim \frac{4A^2 x^2}{\pi^2} \tag{14}$$

Substituting (14) into (13), the corresponding maximum negative temperature gradient is given as

$$\left.\frac{\partial \overline{\tau}}{\partial x}\right|_m \sim -\frac{16}{e\pi^2 x} \tag{15}$$

It can be seen from (14) that the time for the horizontal temperature gradient to reach the maximum value at any offshore distance x approximately corresponds to the time for the thermal boundary layer to reach the local depth, which is $A^2 x^2/k$.

The numerical solutions of the time series of the horizontal temperature gradient for different bottom slopes and offshore distances are plotted together in figure 2(a). In figure 2(b), the horizontal temperature gradient from the numerical simulation is normalised by the maximum negative temperature gradient given in (15), and the time is normalised by the corresponding time scale given in (14). As a consequence, the maximum negative temperature gradient points for different bottom slopes and offshore distances all collapse onto a single point, which demonstrates the validity of the scaling relations (14) and (15).
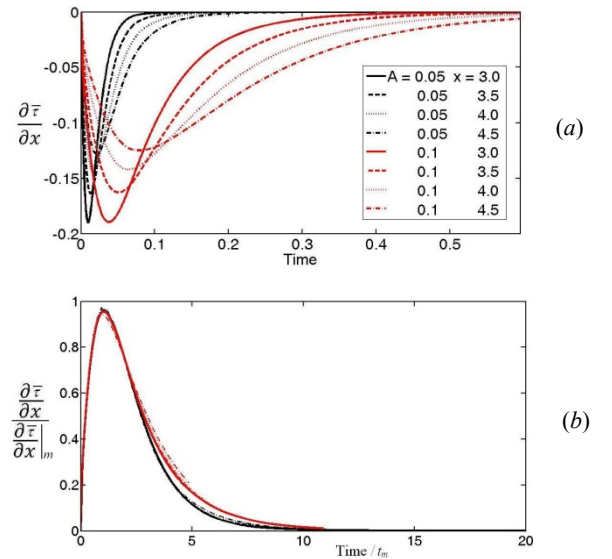

Figure 2. Normalised temperature gradient at various offshore distances and bottom slopes (a) results from numerical simulations (b) numerical results normalized by scaling predictions.

From a spatial perspective, the position where the first derivative of the horizontal temperature gradient (13) with respect to offshore distance x approaches zero is the location where the maximum horizontal temperature gradient occurs at a given time. This location is derived using (13) as

$$x_m \sim \sqrt{\frac{\pi^2 kt}{6A^2}} \sim \frac{\pi}{\sqrt{6}}\frac{\delta_T}{A} \tag{16}$$

The above scale indicates that the maximum horizontal temperature gradient occurs approximately at the position where the edge of the thermal boundary layer intersects with the bottom, which agrees well with the prediction of (14) from a temporal perspective.

The horizontal temperature gradient generates a pressure gradient that drives the flow. A balance between the buoyancy term and the pressure gradient in the vertical momentum equation (3) gives

$$\frac{1}{\rho_0}\frac{\partial p}{\partial y} \sim g\beta(\overline{T} - T_0) \qquad (17)$$

The derivative of (17) with respect to x is obtained as

$$\frac{1}{\rho_0}\frac{\partial^2 p}{\partial x \partial y} \sim g\beta\frac{\partial \overline{T}}{\partial x} \qquad (18)$$

For the horizontal momentum equation (2), the viscous term dominates the inertia and convection terms, and the proper balance is between the pressure gradient and viscous terms:

$$\frac{1}{\rho_0}\frac{\partial p}{\partial x} \sim \nu\frac{\partial^2 u}{\partial y^2} \qquad (19)$$

The derivative of (19) with respect to y is obtained as

$$\frac{1}{\rho_0}\frac{\partial^2 p}{\partial x \partial y} \sim \nu\frac{\partial^3 u}{\partial y^3} \qquad (20)$$

From (18) and (20), a relation between the flow velocity and the horizontal temperature gradient is established as

$$g\beta\frac{\partial \overline{T}}{\partial x} \sim \nu\frac{\partial^3 u}{\partial y^3} \sim \nu\frac{u}{(Ax)^3} \qquad (21)$$

The velocity scale can be derived from (11) and (21) as

$$u \sim 4Rak^2 tA/h^3 e^{-\frac{\pi^2}{4A^2x^2}kt} \qquad (22)$$

A close examination of the above velocity scale indicates that the velocity first increases and then decreases with time, and thus a maximum velocity is reached at a certain point of time. For $t \to \infty$, $u \to 0$, suggesting that for the conduction-dominated region, the flow eventually becomes stationary. The time for the maximum velocity to occur can be derived by setting the time derivative of the velocity (22) to zero. This time is the same as that for the negative horizontal temperature gradient to reach its maximum value, as specified in (14). Substituting (14) into (22), the scale for the maximum velocity is obtained as

$$u_{max} \sim \frac{16}{e\pi^2}Rak\frac{A^3x^2}{h^3} \sim Rak\frac{A^3x^2}{h^3} \qquad (23)$$
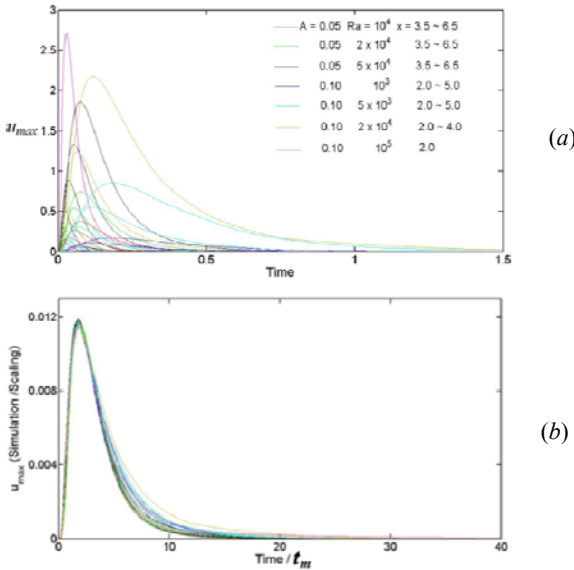
Figure 3. Time series of the maximum horizontal velocity. (*a*) Unscaled numerical data. (*b*) Scaled numerical data.

The time series of the maximum horizontal velocity extracted along vertical lines at different offshore distances are plotted in figure 3(*a*) for different Rayleigh numbers and different bottom slopes. In figure 3(*b*), the numerical data plotted in figure 3(*a*) is normalised using the time scale (14) and the velocity scale (22) respectively. It is clear in figure 3(*b*) that different sets of results from the numerical simulation collapse together at the point of the maximum velocity. Therefore, the dependency of the maximum velocity and its corresponding time on the bottom slope, the Rayleigh number and the offshore distance is well predicted by the scaling relations.

Analysis and simulation for the convective region

From the previous analysis of the conductive region, the maximum flow velocity always occurs at the position where the thermal boundary layer intersects the sloping bottom. For a given time during the flow development stage, the location of the maximum flow velocity can be determined as

$$x_{max} \sim \delta_T/A \sim (kt)^{1/2}/A \qquad (24)$$

For $x > x_{max}$, if convection balances conduction, the thermal boundary layer will stop growing and the flow becomes steady. The balance between convection and conduction is written as

$$u_{max}\frac{T}{x} \sim k\frac{T}{\delta_T^2} \qquad (25)$$

Substituting (11) and (23) into (25), the steady state time scale as a function of the offshore distance x can be derived as

$$t_s \sim \left(\frac{h^3x}{RaAk^2}\right)^{1/2} \qquad (26)$$

Substituting (24) into (26), it can be derived that x_{max} stops moving at a time scale of

$$t_{sc} \sim \frac{h^2}{Ra^{2/3}A^{4/3}k} \qquad (27)$$

Correspondingly x_{max} stops moving offshore at the location of

$$x_{sc} \sim \frac{h}{A^{5/3}Ra^{1/3}} \qquad (28)$$

Substituting (26) into (22), the steady state velocity for the distinct boundary layer, which is also a function of the offshore distance x, can be derived as

$$u_s \sim \left(\frac{Ra \cdot Ak^2x}{h^3}\right)^{1/2} \qquad (29)$$

From (28), a critical Rayleigh number function for the presence of a distinct thermal boundary layer can be derived as

$$f(x) \sim \frac{h^3}{x^3A^5} \qquad (30)$$

The thermal boundary layer is distinct if $Ra > f(x)$. It is seen from (30) that $f(x)$ decreases monotonically with increasing x. A minimum of $f(x)$ occurs at $x = h/A$ for a finite domain with $f(x)_{min} = A^{-2}$. This minimum value determines two distinct flow regimes.

(*i*) For $Ra < A^{-2}$, the entire domain is conduction-dominated and the thermal boundary layer is indistinct at the steady state. The scales for the maximum flow velocity and the corresponding time have been derived and verified. At the steady state, the entire domain becomes stationary and isothermal with a temperature determined by the water surface temperature.

(*ii*) For $Ra > A^{-2}$, the entire flow domain consists of two sub-regions: one with a distinct thermal boundary layer, and the other with an indistinct thermal boundary layer. For a given Ra, the dividing position between the two sub-regions can be obtained from (30) as

$$x_0 \sim h(RaA^5)^{-1/3} \qquad (31)$$

The thickness of the thermal boundary layer at the corresponding location is thus obtained as

$$\delta_d \sim Ax_0 \sim hRa^{-1/3}A^{-2/3} \qquad (32)$$

The steady-state temperature contours for the flow regime of $Ra > A^{-2}$ at two different Rayleigh numbers are shown in figures 4(*a*) and (*b*), in which distinct thermal boundary layers can be identified. It is clear by comparing these two figures that as the Rayleigh number increases, the thickness of the steady-state thermal boundary layer decreases. The thermal boundary layer thickness obtained for different Rayleigh numbers from the numerical simulations is plotted against the scaling prediction (32) in figure 4(*c*). The good linear correlation shown in this figure confirms the scaling prediction.
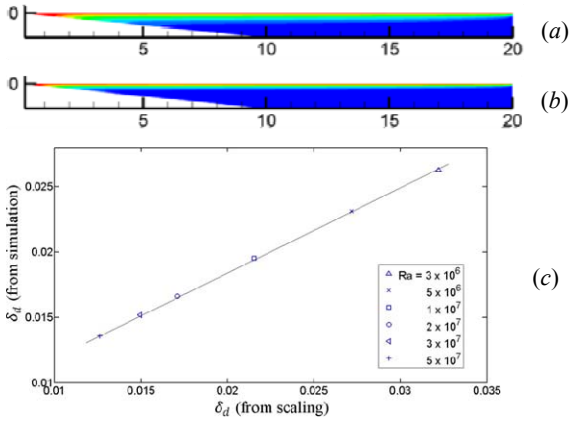
Figure 4. Distinct thermal boundary layer in the convective region. Temperature contours for (*a*) $Ra = 3 \times 10^6$; (*b*) $Ra = 2 \times 10^7$; (*c*) Thermal boundary layer thickness from simulations versus scaling.
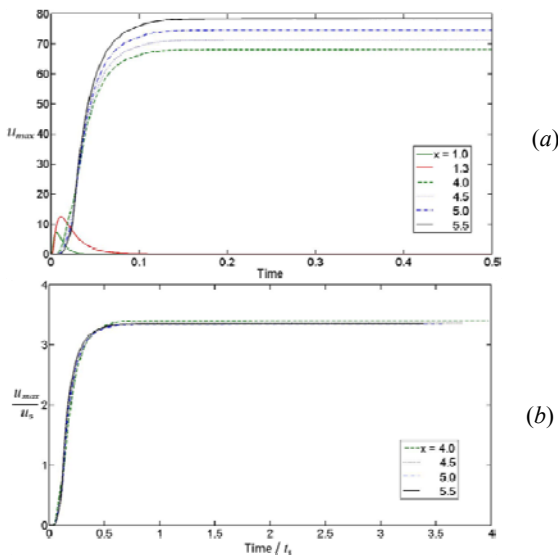

Figure 5. (*a*) Time series of the maximum velocity along the vertical line at different offshore distances for $Ra = 10^6$. (*b*) Time series of the maximum velocity normalized by the steady state scaling.

The time series of the maximum horizontal velocity over the local water depth obtained from numerical simulations at different offshore distances are plotted in figure 5(*a*). It is seen in this figure that, for regions near shore (e.g. $x = 1.0$, 1.3), the velocity first increases with time, and after reaching a maximum value, it decreases to zero, confirming that the flow becomes stationary at the steady state in the conduction dominated region. For the region further offshore (e.g. $x = 4.0$, 4.5, 5.0, 5.5), the velocity first increases with time and then remains constant at the steady state, indicating that convection is strong enough to balance conduction and therefore a steady flow velocity is maintained.

In figure 5(*b*), the time series of the maximum velocity extracted from the offshore regions are replotted after normalisation by the corresponding velocity and steady-state time scales. It is evident that the different time series of the maximum velocity in the regions with distinct thermal boundary layers converge together, confirming the dependence of the scaling predictions on the offshore distance.

Conclusions

Natural convection in a wedge-shaped domain subject to isothermal heating at the water surface is investigated through coupled analytical solution, scaling analysis and numerical simulation. The present study reveals two distinct sub-regions, a conductive region with an indistinct thermal boundary layer and a convective region with a distinct thermal boundary layer.

For the conductive region, theoretical analysis reveals that at any local position the flow reaches its maximum velocity when the thermal boundary layer reaches the local depth. Afterwards, the flow gradually becomes isothermal and stationary as time goes on. The scale of this maximum velocity and the corresponding time for its occurrence are well verified by the numerical simulations. In the offshore region where convection is strong enough to balance conduction, a steady state is reached with a distinct thermal boundary layer. The steady state scales for the convective region are derived and verified.

References

[1] Monismith S.G., Imberger J. & Morison M.L., Convective motions in the sidearm of a small reservoir, *Limnol Oceanogr*, **35**, 1990, 1676–1702.

[2] Sturman J.J., Oldham C.E. & Ivey G.N., Steady convective exchange flows down slopes, *Aquat Sci*, **61**, 1999, 260–278.

[3] Farrow D.E., Periodically forced natural convection over slowly varying topography, *J Fluid Mech*, **508**, 2004, 1–21.

[4] Farrow D.E. & Patterson J.C., The daytime circulation and temperature structure in a reservoir sidearm, *Int J Heat Mass Tran*, **37**, 1994, 1954-1968.

[5] Lei C. & Patterson J.C., Unsteady natural convection in a triangular enclosure induced by absorption of radiation, *J Fluid Mech*, **460**, 2002, 181–209.

[6] Mao Y., Lei C. & PATTERSON J.C., Unsteady natural convection in a triangular enclosure induced by absorption of radiation – a revisit by improved scaling analysis, *J Fluid Mech*, **622**, 2009, 75-102.

[7] Horsch G.M., Stefan H.G. & Gavali S., Numerical simulation of cooling-induced convective currents on a littoral slope, *Int J Numer Meth Fl*, **19**, 1994, 105–134.

[8] Lei C. & Patterson J.C., Unsteady natural convection in a triangular enclosure induced by surface cooling, *Int J Heat Fluid Fl*, **26**, 2005, 307-321.

[9] Mao Y., Lei C. & Patterson J.C., Unsteady near-shore natural convection induced by surface cooling, *J Fluid Mech*, **642**, 2010, 213-233.

[10] Farrow D.E. & Patterson J.C., On the response of a reservoir sidearm to diurnal heating and cooling, *J Fluid Mech*, **246**, 1993, 143–161.

[11] Lei C. & Patterson J.C., Natural convection induced by diurnal heating and cooling in a reservoir with slowly varying topography, *JSME Int J*, *Series B*, **49**, 2006, 605-615.

[12] Bednarz T.P., Lei C. & Patterson J.C., An experimental study of unsteady natural convection in a reservoir model cooled from the water surface, *Exp Therm Fluid Sci*, **32**, 2008, 844-856.

[13] Bednarz T.P., Lei C. & Patterson J.C., An experimental study of unsteady natural convection in a reservoir model subject to periodic thermal forcing using combined PIV and PIT techniques, *Exp Fluids*, **47**, 2009, 107-117.

[14] Patterson J.C. & Imberger J., Unsteady natural convection in a cavity, *J Fluid Mech*, **100**, 1980, 65 - 86.